



Adsorption isotherm and kinetic characteristics of sawdust, shrimp shell, and wild sugarcane-based activated carbon for CO₂ capture

K. Kumaraguru¹ · Panchamoorthy Saravanan¹ · L. Nagarajan² · V. Saravanan³ · R. Rajeshkannan³ · M. Rajasimman³

Received: 12 June 2023 / Revised: 26 October 2023 / Accepted: 5 November 2023

© The Author(s), under exclusive licence to Springer-Verlag GmbH Germany, part of Springer Nature 2023

Abstract

Anthropogenic activities and transportation are primarily responsible for the release of CO₂ into the atmosphere. In this work, waste-based adsorbents are used to capture CO₂ by sorption. Activated carbon was prepared using wild sugarcane and shrimp shells, and it was analyzed using X-ray diffraction, field emission scanning electron microscope, Fourier transform infrared spectroscopies, and X-ray dispersive spectroscopy. Sorption results show a maximum CO₂ uptake of 5.034×10^{-3} mol/g and 4.014×10^{-3} mol/g for the sorbent activated carbon-wild sugar cane shrimp shells (AC-WSSS) and activated carbon-sawdust shrimp shells (AC-SDSS), respectively. Thermodynamic studies of the sorbent AC-WSSS and AC-SDSS were performed and ΔG° (7.45 and 7.48 kJ/mol), ΔH° (13.66 and -48.57 kJ/mol), and ΔS° (38.32 and 36.44 kJ/mol.K) were calculated, and the feasibility of the process was evaluated. The experimental data of the activated carbon isotherm from sawdust and wild sugar cane shells was demonstrated with Langmuir, Freundlich, D-R, Temkin and Sips adsorption isotherm. Higher R^2 (0.9855) value for Langmuir isotherm shows the applicability of the model. The equilibrium point was reached in 80 and 85 min for the prepared biomass AC-WSSS and AC-SDSS, respectively. Desorption results show that the sorbent can be recycled for 3 cycles. It is observed that more than 80% of CO₂ is removed from acetone even after three cycles of desorption experiments. From this work, it reveals that the adsorbent AC-WSSS and AC-SDSS finds to be a better potential for CO₂ capture as adsorbent.

Keywords Activated carbon · Carbon dioxide · Adsorption · Wild sugar cane · Sawdust and shrimp shells · Isotherm and kinetics

Highlights

- CO₂ capture by adsorption can be improved by using activated carbon.
- Sawdust, shrimp shell, and wild sugarcane are considered as a biomass resource.
- Various CO₂ sorption and kinetics studies are discussed.

✉ L. Nagarajan
nagarajan.logu@gmail.com

- ¹ Department of Petrochemical Technology, University College of Engineering-BIT Campus, Anna University, Tiruchirappalli 620 024, India
- ² Department of Biotechnology, Aarupadai Veedu Institute of Technology, Vinayaka Mission's Research Foundation (Deemed to be University), Vinayaka Mission's Chennai Campus, Paiyanoor, Chengalpattu 603 104, India
- ³ Department of Chemical Engineering, Annamalai University, Annamalai Nagar, Chidambaram, India

1 Introduction

Generally, it has been believed that CO₂ is the most significant greenhouse gas (GHG) which contains a greater effect on climatic change [1, 2]. Of all the GHG emissions, CO₂ contributes to 77% which is estimated to be around 400 ppm [3]. It is reported that the first GHG emitted by human activities causing climatic change is CO₂. Due to population increase, there is a necessity for energy which successively demands the burning of fossil fuels and emission of CO₂ into atmosphere [4]. CO₂ is released into the atmosphere by combustion of fuel like gas, coal, and industrial processes that has oil refining, cement manufacturing, iron and steel, and thermal power plants. To scale back the emission of CO₂ from combustion of fossil fuels in atmosphere and reducing heating, separation of CO₂ and its capture is gaining importance in recent days [5]. CO₂ emission may be a major contributor for global warming, and it creates a widespread awareness in recent days. Power and transport sector

contributes 33% and 14% of CO₂ emission, respectively. The global yearly temperature has risen by a little more than 1 °C, or roughly 2 °F, during the Industrial Revolution. It increased by 0.07 °C (0.13 °F) in every 10 years between 1880 and 1980, when the accurate record keeping started. Since 1981, the rise is more than doubled: the global annual temperature has risen by 0.18 °C (0.32 °F) in each decade of the last 40 years. The current trend indicates that rising carbon dioxide (CO₂) levels in the atmosphere constitute a severe threat to global issues, with unusual phenomena expected to occur [6]. If proper action is not initiated to curb CO₂ emissions, it is going to cause rise in mean temperature level and negative impact on biotic environment. Natural ecosystems are subjected to endangerment with emission of CO₂ into atmosphere. Various forms are adopted for permanent storage of CO₂. These forms include gaseous storage in various deep geological formations and solid storage including saline-exhausted gas fields by the reaction of CO₂ with metal oxides to provide stable carbonates. Many methods were suggested and are in practice for capturing CO₂ that features pre-oxy-fuel and post-combustion techniques. Because of the business opportunity of CO₂ and as a resource, it is beneficial in both environmental and economic view point [7].

Biomass energy conversion combined with carbon capture and storage can help to reduce CO₂ levels in the atmosphere [8]. Absorption, adsorption algal bio-fixation, membrane separation, and cryogenic separation are a number of the mostly applied technologies for CO₂ removal. After a lot of research and testing, it was discovered that capturing CO₂ adsorption is effective [9]. In current scenario, adsorption seems to be a really promising mechanism, extensively employed for gas treatment because of its easier operation, economy, energy saving, good transference capacity, appreciable multifaceted tendency, and, if combined with a good regeneration process, in the absence of byproducts [10]. Adsorption is the phenomenon of attachment of gas or liquid on to a solid surface. Success of adsorption process depends on durability and regenerating tendency of adsorbent.

Sorbents such as zeolite, crystalline porous solids, polymers, activated carbon, and metalliv aluminosilicates are well-known [11]. Various researchers investigate the adsorbent preparation from agricultural and biomass wastes and shown its application for CO₂ adsorption [12]. Graphene has been discovered to have the higher surface area of any activated carbon material, with a surface area of roughly 3335 m²/g [13, 14] because it has the disadvantages of being expensive, difficult to synthesize, and, most importantly, harmful to health. Various forms of adsorbents are available in market which includes activated carbons, silica gel, zeolites, metal oxides, metal organic frame works, surface-modified C intermediate temperature sorbents [11, 15–17]. Higher CO₂ uptake is facilitated by (activated carbon) AC,

zeolites, and MOFs. Since these sorbents are expensive, it becomes necessary to regenerate. AC is relatively better than the others because of higher uptake of CO₂ at ambient pressure, affordability, and simple to regenerate. AC is employed during this work as adsorbent for adsorbing CO₂ because it has the characteristics like high adsorption, lesser cost, high hydrophobicity, and low energy requirement for its restoration to its original form [18–21].

Activated carbon is typically prepared by heating at higher temperature for achieving desired activating level [22]. Presence of high lignocellulose content AC is ready from organic biomass. Activation by chemical methods is analogously better than physical methods for various reasons like less activation time, comparatively better yield and bigger micro pore volume [23]. Because of inherent dehydrogenation properties and fewer tar formation, well-defined pore structures may be prepared from lignocellulosic materials with oxyacid and caustic soda as activating agents [24]. By varying the ratios of activating agents and biomasses in chemical activation method, final AC properties may be improved to a bigger extent. Adsorbent prepared from shrimp shell-derived chitosan is found to have good specific area and better adsorption capacity [17]. Sawdust also found to be an inexpensive source and proves to own good adsorption capacity [25]. Hence, these materials are selected as a source for the preparation of sorbents.

Still research is in progress in order to find economic and effective sorbents for CO₂ sorption. Hence, the objective of this work is to develop a new sorbent, by combining shrimp shell and sawdusts for the sorption of CO₂. Dehydration, carbonation, and activation are the three steps used to transform wild sugarcane and shrimp shell into activated carbon. It was found that the ratio of higher cellulose to lower lignin and hemicelluloses in wild sugarcane is 2:1:1, resulting in a microporous structure on activated carbon [26–28].

2 Materials and methods

2.1 Reagents

Chemical reagents viz. phosphoric acid and hydrochloric acid were procured from Sigma-Aldrich. Biomasses from wild sugar cane bagasse dust and shrimp shells are prepared by combustion method. Five gas analyzer set up for gas analysis were employed.

2.2 Sorbent material preparation

2.2.1 Synthesis of sawdust and shrimp shells

In this study, sawdust (SD) was obtained from the construction sites at Kodungaiyur (13.1375° N, 80.2478° E),

Chennai, Tamil Nadu, India. Shrimp shell (SS) was taken from sea shore of Ennore 13.2175° N, 80.32155° E, Thiruvallur, Tamil Nadu, India. As a pre-synthesis process, SD and SS were taken in the ratio of 1:1 and washed with distilled water and then dried. The dried samples are then crushed and soaked in HCl in the ratio of 1:1.5 for 6.5 h. Then, it is washed in tap water and distilled water, until its pH reaches neutral. After drying, it is impregnated with phosphoric acid in the ratio of 1.5:2.25 and soaked for 10 h. Then, it is washed in distilled water till the pH reaches neutral. The dried material is kept in muffle furnace at a temperature of 500 °C for 50 min. The sample thus obtained is activated carbon-sawdust shrimp shells (AC-SDSS).

2.2.2 Synthesis of wild sugarcane and shrimp shells

Wild sugarcane (WS) was collected near the marshy lands of Perumalpattu (13.0999° N, 79.9920° E) in the Thiruvallur district of Tamil Nadu for this study. Shrimp shell (SS) was collected at the seashore of Ennore, Thiruvallur, Tamil Nadu, India, at 13.2175° N, 80.32155° E. As part of the pre-synthesis procedure, WS and SS were rinsed in distilled water and dried before being crushed and steeped in HCl in the ratio of 1:1.25 for 7 h. Then, it is cleaned in tap and distilled water until the pH is balanced. After drying, it is impregnated with 1.5:2.0 phosphoric acid and steeped for 11 h before being washed in distilled water until the pH reaches neutral. For 60 min, the dry material is maintained in a muffle furnace at a temperature of 580 °C. The dried material is the activated carbon-wild sugar cane shrimp shells (AC-WSSS).

2.3 Experiments on adsorption and sorbent studies

In this work, CO₂ gas is considered as adsorbate, and biomass prepared from sawdust and shrimp shell (AC-SDSS) is used as adsorbent. Batch experiments are carried out in 500-ml conical flask fitted with an air tight rubber cock. The adsorbent is kept in conical flask and degassed for 3.5 h using nitrogen gas to remove impurities from adsorbent, and it is cooled to reach the room temperature. CO₂ from cylinder is allowed to pass through rubber tubing to conical flask in which adsorbent is taken by means of valve between cylinder and conical flask at a controlled rate, and a set of experiments is conducted using five gas analyzer set up. A study on the effect of various parameters such as adsorbent dosage, flow rate or concentration, and contact time are conducted, and the amount of CO₂ adsorbed is calculated.

CO₂ is purged over the prepared adsorbent using a gas analyzer set up. The concerned adsorbent is placed on a 500-ml conical flask and degassed under vacuum for specific time before CO₂ adsorption to ensure that the impurities are removed from them. Contact is made between adsorbent and

CO₂ by allowing the valve between cylinder and conical flask open in a controlled manner. Arai Model EPM 1601 a compact multi-component gas analyzer with an integrated sample conditioner and probe stinger suitable for process, compliance monitoring, and reporting is used. With change in parameters, the amount of CO₂ adsorption is calculated. Firstly, a fixed quantity of adsorbent is taken in conical flask, by varying the gas concentration and fixing the time of contact; the amount of CO₂ adsorbed is calculated. In second case, the adsorbent dosage is varied and the concentration of CO₂ is fixed, and time of contact is varied and the amount of CO₂ adsorbed is calculated. In third case, the adsorbent dosage is varied by keeping the concentration of CO₂ and time of contact as fixed; the amount of CO₂ is calculated. It is illustrated in Fig. 1.

2.4 Physicochemical characterizations

The work was carried out using an FEI Quanta 450 FEG field emission scanning electron microscope with an EDS detector and a 5 kV accelerating voltage. Optical contact angle 15EC equipment was used to acquire images of static and dynamic contact angles. Each measurement was taken five times, with the average of the static contact angle values being used to determine the actual contact angle. In transmittance mode, an ATR-RX1 spectrometer (PerkinElmer, USA) was utilized to record the Fourier transform infrared (FTIR) spectra. All recorded spectra were obtained using PerkinElmer scan spectra accumulation in the wave number range of 400–4000 cm⁻¹ with a resolution of 3.0 cm⁻¹. The XRD study of prepared AC-SDSS was acquired by X-ray diffraction (XRD, Philips, the Netherlands) at a voltage of 30 kV and a current of 35 mA. In the range of 5 to 90°, a collimated angle of 2 was adjusted.

2.5 Sorption equilibrium isotherm

The batch experimental data was applied to linear isotherms namely Langmuir, Freundlich, Dubinin-Radushkevich, Temkin, and Sips isotherms to determine the mechanism of CO₂ adsorption onto various adsorbents AC-WSSS and AC-SDSS.

2.6 Thermodynamic study of adsorption process

The effects of the temperature on the adsorption of CO₂ on various adsorbents were studied in the range of 303 to 323 K at the optimum conditions.

2.7 Sorption kinetics

Adsorption kinetics was checked with I order and II order models. The experimental values and predicted values are expressed in terms of R^2 .

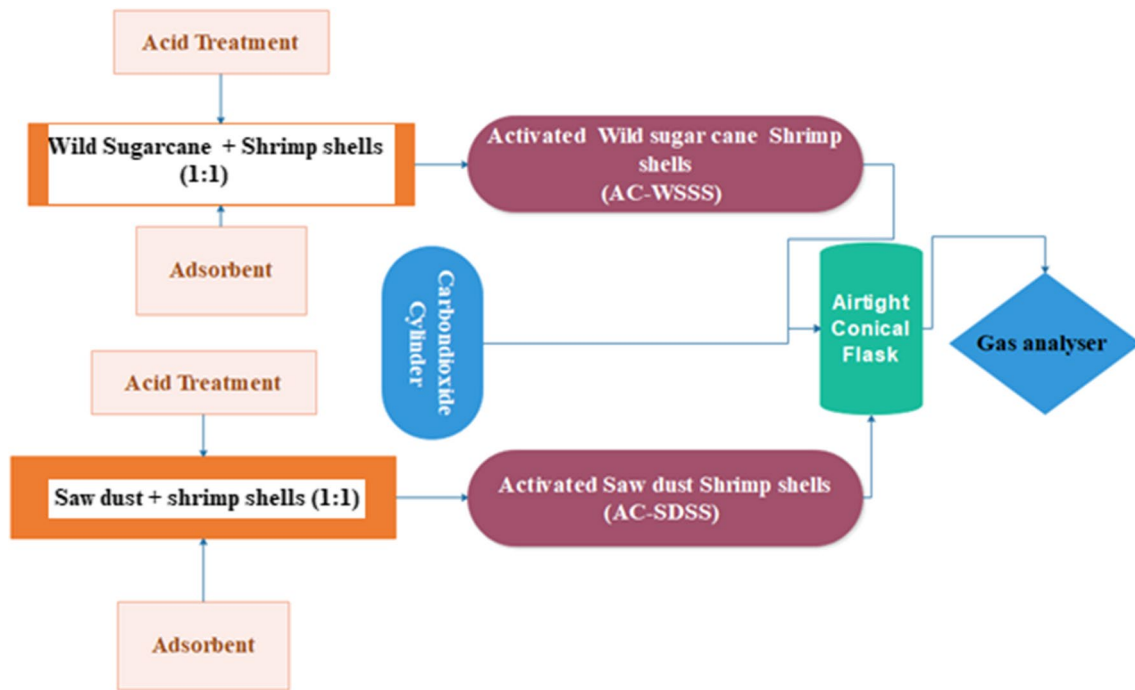


Fig. 1 Experimental setup for CO₂ adsorption

3 Theory/calculation

3.1 Sorption studies

Percentage adsorption of CO₂ is calculated by the following equation.

$$\text{Percentage Adsorbed} = \frac{C_0 - C_e}{C_0} \times 100 \quad (1)$$

where C_0 and C_e are initial and final gas phase concentration of CO₂ (g/L/min), respectively. Kinetics studies are performed with fixed concentration of CO₂ (4×10^{-4} , 5×10^{-4} , and 6.0×10^{-4} M) using the adsorbent for various intervals of time starting from 10 to 100 min in steps of 10 min. Saturation point was attained at 80th and 85th min for the prepared biomass with sawdust, shrimp shells and wild sugar cane, shrimp shells, respectively.

The amount of CO₂ adsorbed is calculated by using the following equation.

$$\text{Amount Adsorbed } q_t = C_0 - C_t \times \frac{V}{M} \quad (2)$$

q_t is the amount of CO₂ adsorbed (mol/g/min), C_0 and C_t are concentrations of CO₂ M (g/L/min) at initial and final time t (min), respectively. V is the volume of CO₂ (L/min) and m is the mass of adsorbent added (g).

Regeneration of CO₂ and reusability of AC-SDSS and AC-WSSS as adsorbent were carried out by taking CO₂ of concentration 5×10^{-4} M and adsorbent dose of 0.150 g. The percentage desorption of CO₂ was obtained using the equation.

$$\text{Percentage desorption} = \frac{\text{Concentration of desorbed CO}_2}{\text{Concentration of adsorbate loaded on AC - SD}} \quad (3)$$

Acetone was found to be efficient than ethanol. Hence, desorption studies are conducted using acetone.

3.2 Sorption isotherm models

3.2.1 Langmuir adsorption isotherm

It is fitted with Langmuir adsorption, and its equation is as follows:

$$\frac{C_e}{q_e} = \frac{1}{Q_m K_L} + \frac{1}{Q_m} \quad (4)$$

Langmuir (1916) isotherm is applied for determining the applicability of adsorbent for CO₂ adsorption by using dimensionless constant known as separation factor [29].

$$R_L = \frac{1}{1 + K_L C_0} \quad (5)$$

R_L between 0 and 1 in this study is a positive sign of better CO₂ adsorption on adsorbent.

3.2.2 Freundlich adsorption isotherm

The equation governing Freundlich adsorption isotherm [30] is as follows:

$$\log q_e = \log K_F + \frac{1}{n} \log C_e \quad (6)$$

q_e and C_e are the same as in Langmuir adsorption isotherm, and “ n ” is a dimensionless constant for a given adsorbate and adsorbent concentration at particular temperature. It is observed that Freundlich adsorption isotherm is empirical in nature, and it assumes that the adsorbent surface is heterogeneous. K_F and n values are calculated from slope and intercept of plot between $\log q_e$ and $\log C_e$.

3.2.3 Dubinin–Radushkevick adsorption isotherm

D-R model is used for explaining adsorption processes onto heterogeneous surfaces with Gaussian energy distribution [20]. It is dependent on temperature as suggested by Sevilla and team [31]. In this model, Q_m is the adsorption capacity, E is the characteristic energy of adsorption, and ε is the D-R isotherm coefficient. The D-R equation is as follows:

$$\ln q_e = \ln Q_m - K\varepsilon^2 \quad (7)$$

3.2.4 Temkin adsorption isotherm

In Temkin isotherm model, the effects of indirect adsorbate and adsorbing species on the adsorption process are taken into consideration. This isotherm model is valid only for an intermediate range. The linear form of Temkin isotherm model is given by Parshetti and coworkers [31]. Its equation is as follows:

$$q_e = \frac{RT}{b} \ln A_T + \frac{RT}{b} \ln C_e \quad (8)$$

3.2.5 Sips adsorption isotherm

The combined form of the Langmuir and Freundlich models is the Sips adsorption isotherm model. From the Sips adsorption equation, q_m is the maximum adsorption capacity, b is the Langmuir constant that is related to the apparent energy of sorption, and in “ n ,” the Freundlich exponent is calculated [32].

$$q = \frac{q_m (bp)^{\frac{1}{n}}}{1 + (bp)^{\frac{1}{n}}} \quad (9)$$

3.3 Thermodynamic study of adsorption process

From Van't Hoff equation, standard enthalpy and entropy were determined as suggested by Murie Dwiyanti and team [12]. From the plot of $\ln K$ Vs $1/T$, slope and intercept give ΔH° and ΔS° values. It is listed in Table 3. At 303 K, 313 K, and 323 K, the effect of temperature on adsorption of CO₂ on AC-SDSS was calculated.

$$\ln K = \frac{\Delta S^\circ}{R} - \frac{\Delta H^\circ}{RT} \quad (10)$$

$$\Delta G = -RT \ln k \quad (11)$$

R denotes the universal gas constant (8.314 J/mol/K) in Eqs. 10 and 11, and T indicates the adsorption temperature in Kelvin.

3.4 Sorption kinetics

Fast adsorption kinetics is one of the most important features expected of a good adsorbent because the residence time necessary to complete the adsorption process, adsorption bed size, and, as a result, unit capital expenditures are all integrally linked to the rate of adsorption. For example, the pseudo-first order model overestimates CO₂ uptake in the early phases of adsorption and underestimates it as the equilibrium approaches. Nonetheless, the pseudo-first order prediction closely follows the patterns of the experimental data during the last phases of adsorption, and the equilibrium CO₂ adsorption capacities are in good agreement with the experimental values.

The pseudo-second order model, on the other hand, overestimates CO₂ uptake in the early stages while underestimating it in the latter stages since it predicts considerably lower equilibrium adsorption capabilities than the experimental values. Diffusion-based effects may be highly essential for porous adsorbents like activated carbons; hence, the physical relevance of the evaluated rate constants must be carefully determined to acquire an accurate understanding of the mass transfer mechanisms involved. Using an intra-particle diffusion model, the possibility of intra-particle diffusion resistance affecting CO₂ adsorption on the evaluated activated carbons was investigated.

The conformity of the experimental work and kinetic model can be analyzed by the regression coefficient (R^2) values [33]. Lagergren's pseudo-first-order and pseudo-second-order models were used to test the kinetic behavior in this work, and the regression coefficient (R^2) values can be used to analyze the conformity of the experimental work and kinetic model. The results of the kinetic tests were used to Lagergren-Svenska and Ho-pseudo-first-order McKay's

(PFO) and pseudo-second-order (PSO) models [34, 35]. The following are the PFO and PSO equations, respectively.

Equation (10) can be used to define the linearized Lagergren pseudo-first-order model, where q_e and q_t are the quantity of CO_2 adsorbed in ($\text{mg}\cdot\text{g}^{-1}$) at equilibrium and time t , respectively, and k_1 is the pseudo-first-order model's rate constant (min^{-1}). In addition, Zafanelli and team [36] used Eq. 11 to calculate the pseudo-second-order model and starting rate of adsorption, h ($\text{mg}\cdot\text{g}^{-1}\text{min}^{-1}$).

A plot of $1/q_t$ against time (t) will result in a straight line with $1/h$ and $1/q_e$ as the y-intercept and slope, respectively, if the pseudo-second-order kinetic model is applicable in the adsorption process.

Equation 12 [37, 38] can be used to explain the intra-particle diffusion model, where q_t represents the amount of CO_2 adsorbed at any time t ($\text{mg}\cdot\text{g}^{-1}$), k_{id} represents the intra-particle rate constant ($\text{mg}/\text{min}\ t^{1/2}$), and t represents the contact duration ($\text{min}^{1/2}$). When the adsorption process obeys the intra-particle diffusion model [37], a straight linear plot that passes through the origin is observed.

$$\log(q_e - q_t) = \log q_e - \frac{K_1 t}{2.303} \quad (12)$$

$$\frac{t}{q_t} = \frac{t}{K_2 q_e^2} + \frac{1}{q_e} \quad (13)$$

$$q_t = K_{id} t^{0.5} + C \quad (14)$$

4 Results and discussion

4.1 Physicochemical characterization on sorbent materials

4.1.1 Textural properties of AC-SDSS and AC-WSSS

The pore volume of the adsorbent is determined using BET analysis, which gives clear indication of their adsorption capacity and nature of adsorbents [39, 40]. The results of BET analysis and iodine value are given in Table 5. The adsorption capacity of activated carbon is quantified by the iodine value. The surface area of activated carbon was determined using the Brunauer-Emmet-Teller (BET) method using a Quantachrome NovaWin instrument and degassing nitrogen for 4 h [41]. Using the BET equation, the specific surface area of AC-SDSS was found to be roughly $1035\text{ m}^2/\text{g}$. The distribution of pore size has been determined using the Barrett-Joyner-Halenda (BJH) method. MAC had a pore size of 1.748. Using the BJH method, the pore volume was $0.43\text{ cm}^3/\text{g}$, showing the mesoporous nature of synthesized AC-SDSS [42]. The iodine concentration was $960\text{ m}^2/\text{g}$.

AC-WSSS has a higher surface area of $1310\text{ m}^2/\text{g}$; its values are shown in Table 1.

4.1.2 Elemental composition

EDX is an X-ray technique for determining a material's elemental composition. In AC-WSSS, the raw, non-functionalized, and functionalized activated carbons are consisting of C, O, and K, according to elemental analyses (given in Fig. 2). The content of C increased dramatically from 58 to 79% after the raw material was activated. After adsorption, the carbon content increased by around 69 to 81%. Because heat supply during activation commences thermal degradation, volatile matter is eliminated, and a stable carbon element is kept; this finding demonstrated that the activation process aided enhance C composition [36]. Phosphorus was found in non-activated carbon, indicating a reaction with phosphoric acid during the impregnation process; as a result, more active sites for CO_2 adsorption become available, and CO_2 collection is improved [43]. According to the elemental analysis, the carbon/oxygen ratio has increased from 1.65 to 2.43, indicating that the carbon content has increased, and this is shown in Fig. 2.

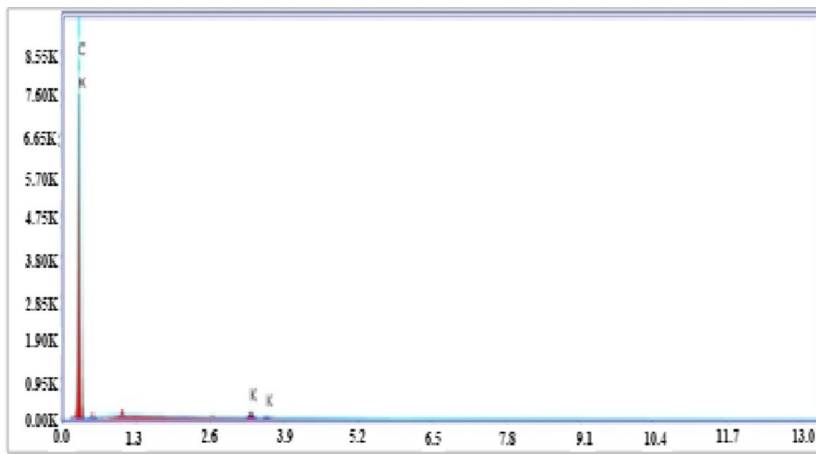
By comparing the elemental analysis of sawdust-based activated carbon, before and after adsorption, it is seen that the carbon ratio increased. This suggests that there is interaction of CO_2 on the surface of the activated carbon (adsorption takes place). It is shown in Fig. 3a and b.

4.1.3 Surface morphology

FESEM of AC-WSSS before and after CO_2 adsorption The sharp and projecting morphology at the pore borders can sometimes cause second electron charge accumulation and form a bright edge on the periphery of black pores, resulting in an underestimation of pore percentage. The variability and PSD properties in small scale can be qualitatively

Table 1 Property of AC-SDSS and AC-WSSS

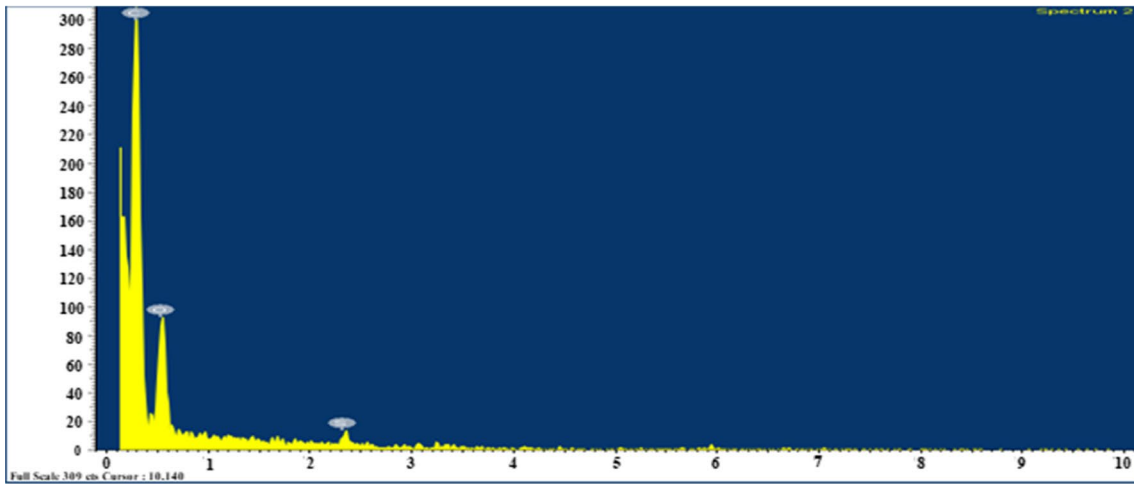
Parameter	AC-WSSS	AC-SDSS
Yield (%)	19.2	18.5
Burn off (%)	10.4	9.6
Surface area (m^2/g)	1310	1035
pH	8.3	7.9
Moisture content (%)	9.3	8.8
Ash content (%)	4.2	4.8
Pore volume (g/cm^3)	0.73	0.71
Pore size	1.712	1.812
Volatile matter (%)	77.2	78.9
Fixed carbon content (%)	17.9	18.2
Iodine value (m^2/g)	1415	960



Loc: 50.0 0 Counts 0.000keV Det: Octane Ultra

C K	69.2	75.7	2118.2	2.7	0.5919	0.7478	1.1437	1.0000
O K	28.4	23.3	683.2	7.4	0.0938	0.7209	0.4578	1.0000
S K	2.4	1.0	149.0	5.2	0.0168	0.6688	1.0375	1.0103

(a)



Full Scale: 309 ch. Cursor: 10.140

Element	Weight%	Atomic%
C K	81.64	88.48
O K	17.20	11.04
S K	1.16	0.48
Totals	100.00	

(b)

Fig. 2 EDS of AC-WSSS before (a) and after (b) CO₂ adsorption

examined under low magnification. Pixel counts can be used to calculate the quantity and types of pore and component types at higher magnification [44]. The properties of AC-WSSS are analyzed using scanning electron micrographs and are shown in Fig. 4a and b.

At other sites, activated carbon made from wild sugar cane and sawdust with brighter patches was coated. By comparing micrographs taken before and after adsorption, it can be shown that the cubes in the AC-WSSS structure were converted to particles due to CO₂ adsorption by carbon materials. When examining the morphology of the CO₂ and AC-WSSS illustrated in Fig. 4, it is evident that chemical adsorption is involved.

FESEM of AC-SDSS before and after CO₂ adsorption Figure 5a shows the low and high magnification morphology of AC-SDSS. It looks like sheets and bundles of pipe-like structures [45]. From Fig. 5b, it is observed that activated carbon sheets are of micron size, and there is a little change in morphology after interaction with CO₂ molecules. In the sample after adsorption, there seems to be some chemical change involved in the material.

4.1.4 Functional groups

Electromagnetic radiation can be absorbed, transmitted, reflected, and dispersed or exhibit photoluminescence (PL), which can reveal a lot about a substance's molecular structure and energy level transition [46, 47]. When paper samples are placed in the direction of an infrared beam, they absorb and transmit light, and the light signal then passes through the sample and into the detector. The detector monitors the amount of radiation that enters a sample as well as the amount of radiation that passes through it. A computer converts its output as a function of time into a plot of absorption against wavenumber using the Fourier transform method [47].

Figure 6 shows the FTIR spectra of CO₂ before and after adsorption on AC-SDSS surface. The IR band observed between 3000 and 3500 cm⁻¹ related to O–H stretching vibrations, and the peak at 2921 cm⁻¹ indicates the presence of alkanes and C–H stretching vibration. The peaks between 1650 and 1500 cm⁻¹ correspond to amide carboxyl group C=O, and the peaks between 1400 and 1420 cm⁻¹ indicate C=C groups present in carbon. Peak at 1130 cm⁻¹ corresponds to carboxylic acid C–O at the surface of adsorbent. As there is a peak shift after adsorption seen in the FTIR, it confirms that it follows chemisorption.

Figure 7 shows the Fourier transform infrared spectroscopy (FTIR) spectra of CO₂ adsorption on AC-WSSS before and after adsorption. The surface functional groups of produced activated carbon were characterized using

FTIR spectra. The porosity of activated carbon as well as the chemical reactivity of functional groups at the surface influences its adsorption capacity [48]. The presence of distinct functional groups on the carbon surface contributes to different molecule species preferentially adsorbing carbon [49]. The large adsorption peak at 3438 cm⁻¹ could be attributed to intermolecular hydrogen bonding of polymeric substances such as alcohols, phenols, and carboxylic acids, indicating the presence of free hydroxyl groups on the activated carbon surface [50].

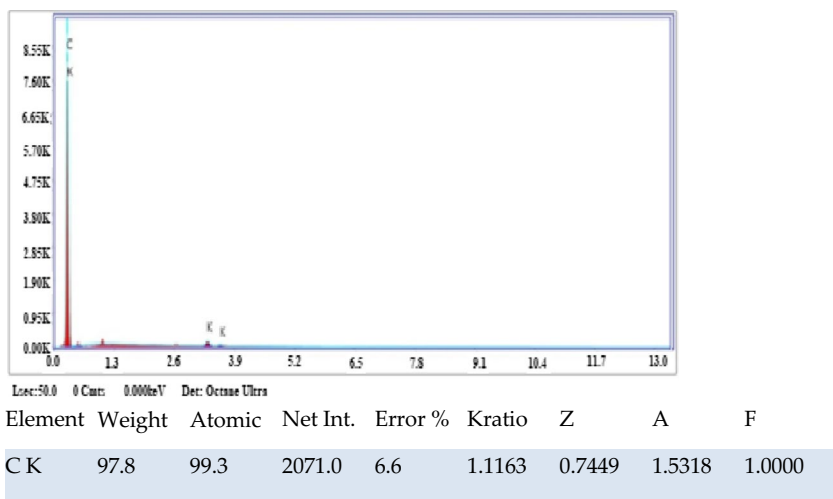
Similarly, the carbonyl C=O stretching vibration in aldehydes, ester or ketones, and carboxyl group corresponds to the peak at 1627 cm⁻¹ and 1588 cm⁻¹ [50]. The strong bands at 2921 cm⁻¹ are the bending vibrations of the C–H group, which may be found in alkyl groups. The presence of oxygen-containing surface functional groups such as hydroxyl groups, carboxyl groups, and carbonyl groups is shown by the FTIR spectra. These deductions lead to the conclusion that the adsorbent was thermally stable during adsorption.

4.2 Adsorption characteristics of CO₂ on AC-SDSS and AC-WSSS

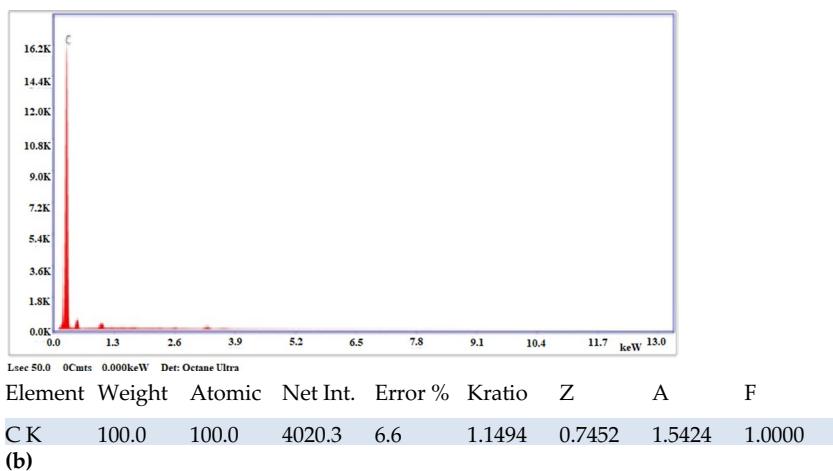
4.2.1 Effect of adsorbent dosage

The effect of adsorbent dosage is investigated by fixing the concentration of CO₂ at 5 × 10⁻⁴ M. Increasing the adsorbent dosage from 0.05 to 0.2 g for AC-SDSS, the percentage of CO₂ adsorbed increased from 78.9 to 90.8% up to a certain point then it got saturated. An optimum adsorbent dosage was found to be 0.150 g. The results are depicted in Fig. 8. The BET surface area of AC-SDSS is 1035 m²/g which attributes for better adsorption. With decrease in effective surface area, the adsorption decreases [40]. Similarly, for AC-WSSS, to determine the effect of adsorbent dosage, the CO₂ concentration was set at 5 × 10⁻⁴ M, and the adsorbent dose was changed in increments of 0.030 g from 0.030 to 0.210 g. As the AC-WSSS dosage is increased, the percentage adsorption of CO₂ increases until it reaches a saturation point. The AC-WSSS has a BET surface area of 1310 m²/g, indicating that adsorption increases from 82.3 to 92.4% as dosage increases. The adsorbent dosage that works best is 0.150 g. CO₂ adsorption was shown to decrease as the adsorbent dosage was further increased as suggested by Stephen and Yusuf in their work [51]. This is due to the fact that partial aggregation of biomass at higher biomass concentrations reduces the effective surface area available for sorption [44]. It is depicted in Fig. 8.

Fig. 3 EDS of AC-SDSS before (a) and after (b) CO₂ adsorption



(a)



(b)

4.2.2 Effect of CO₂ concentration

For AC-SDSS, the adsorbent dosage was fixed at 0.150 g,

and the concentration of CO₂ is varied from 1 × 10⁻⁴ to 10 × 10⁻⁴ M. The percentage adsorption of CO₂ dropped from 91.22 to 79.3% as concentration increased, due to

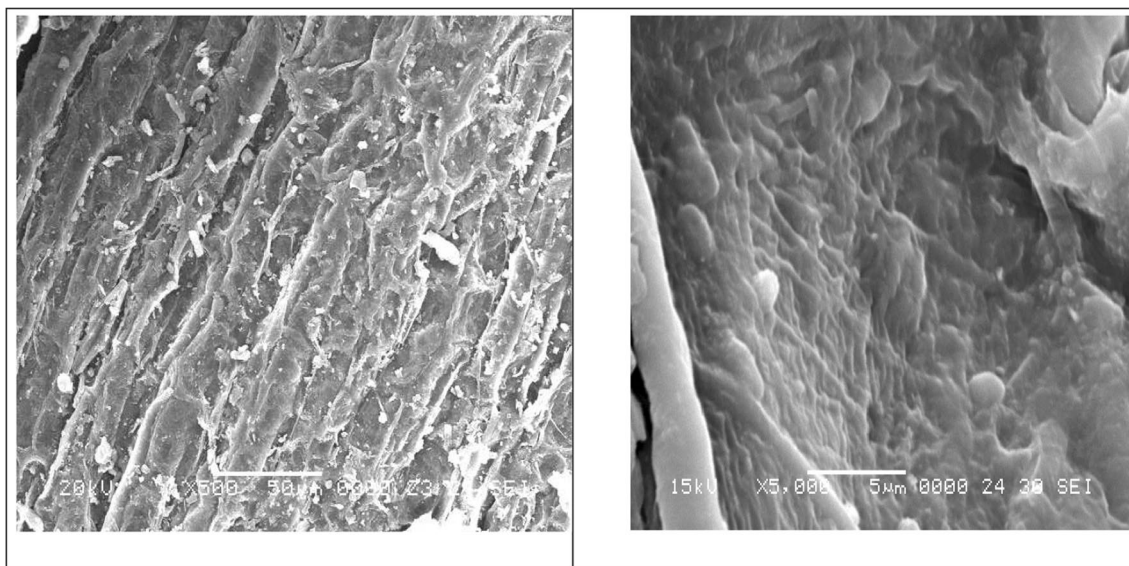


Fig. 4 FE-SEM images of AC-WSSS before and after CO₂ adsorption

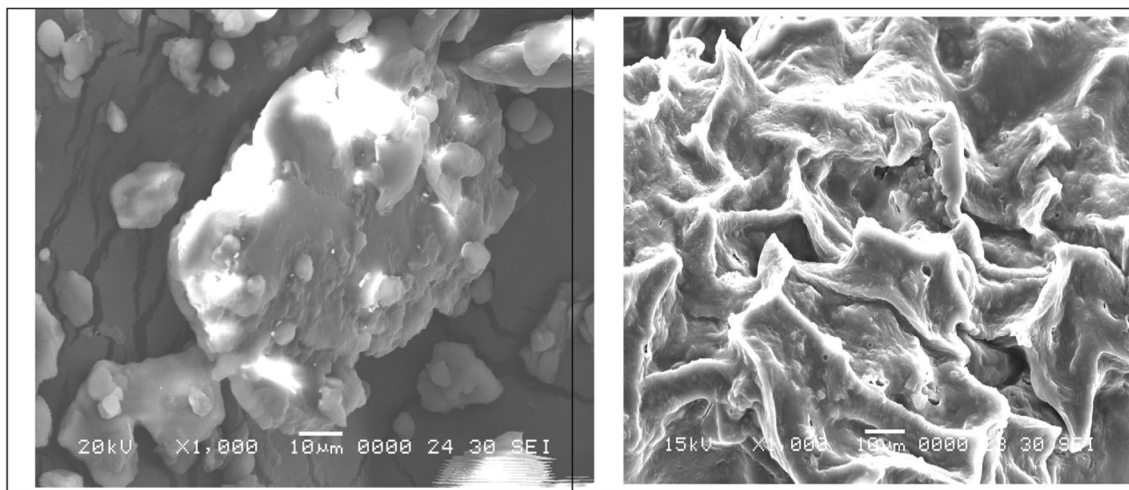


Fig. 5 a FE-SEM images of AC-SDSS before CO₂ adsorption. b FE-SEM images of AC-SDSS after CO₂ adsorption

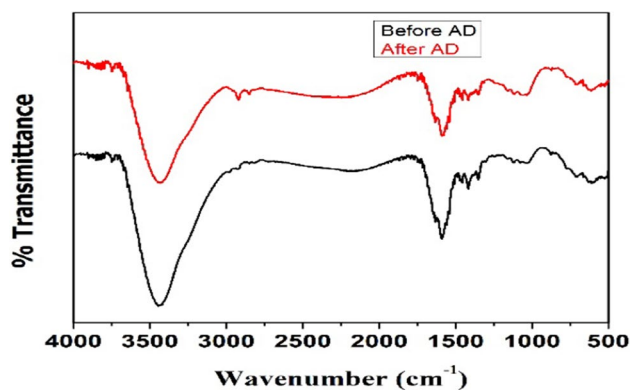


Fig. 6 FTIR of AC-SDSS before and after CO₂ adsorption

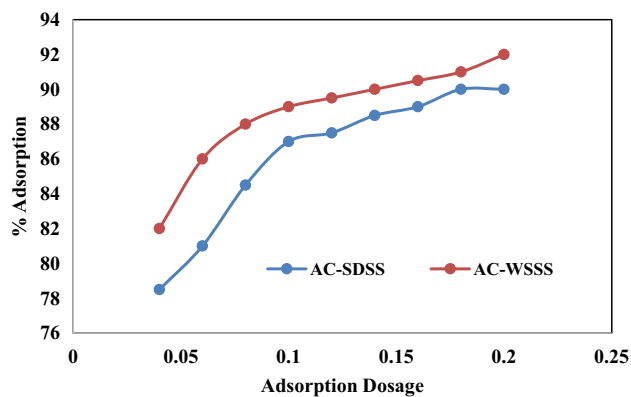


Fig. 8 Effect of adsorbent dosage on adsorption of CO₂ using AC-SDSS and AC-WSSS

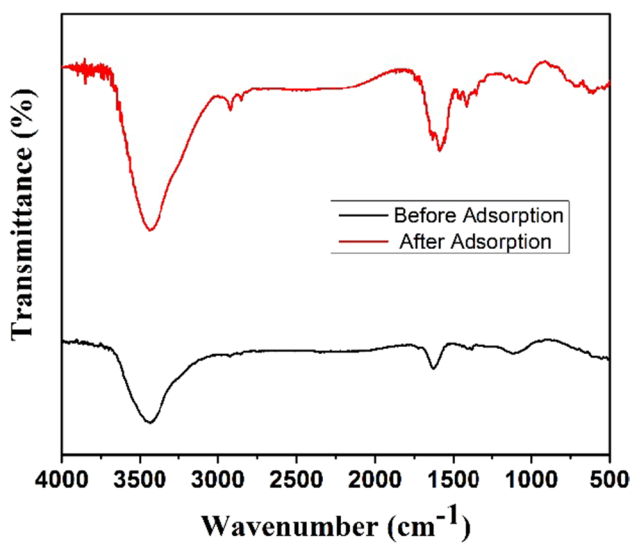


Fig. 7 FTIR of AC-WSSS before and after CO₂ adsorption

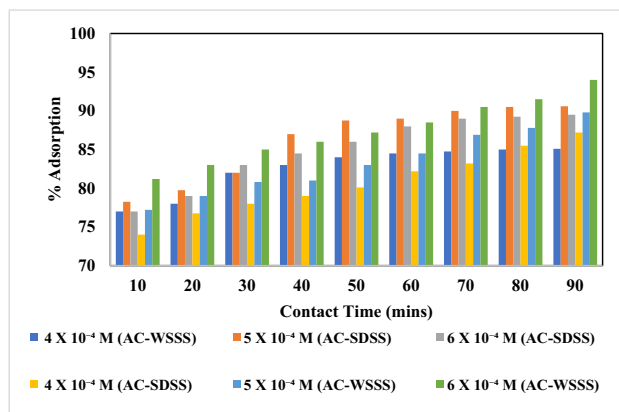


Fig. 9 Effect of contact time on adsorption of CO₂ for AC-SDSS and AC-WSSS

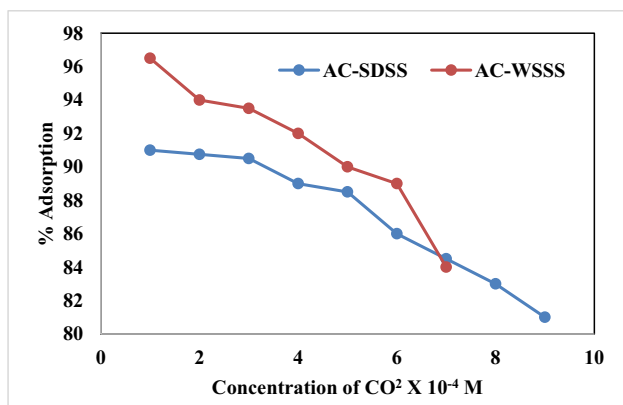


Fig. 10 Effect of concentration on adsorption of CO₂ for AC-SDSS and AC-WSS

unavailability of adsorption sites as CO₂ concentration increased (Fig. 9). In this study, adsorption slowly increases and reaches maximum at 5 × 10⁻⁴ M as more sites are available for CO₂ molecule to settle in and get adsorbed after which the available sites get clogged up due to increase in concentration [40, 52]. This is depicted in Fig. 10. Similarly, experiments were performed using AC-WSS. With increasing CO₂ concentrations, the percentage adsorption of CO₂ falls. Figure 10 reveals that the adsorption capacity has reduced from 95.3 to 86%, indicating that adsorption sites on the adsorbate have become scarce as CO₂ concentration increases. Increasing concentration increases the interaction between CO₂ and adsorbent surface as inferred by Arunaporn and Patcharin [53]. As the surface of the adsorbent is loaded with CO₂, adsorption diminishes as the dosage of the adsorbent increases [54]. At a concentration of 4 × 10⁻⁴ M, adsorbent dose of 0.15 g and contact duration of 55 min, maximum adsorption occurs using AC-SDSS whereas

for AC-WSS, the maximum sorption occurs at 5 × 10⁻⁴ M and adsorbent dosage of 0.15 g and contact time of 55 min.

4.2.3 Effect of contact time of CO₂

By varying the concentration of CO₂ (4 × 10⁻⁴ M, 5 × 10⁻⁴ M, and 6 × 10⁻⁴ M) and keeping adsorbent dosage at 0.150 g, the experiment was performed at different contact time from 10 to 90 min. It was found that a contact time of 80 min and at a concentration of 5 × 10⁻⁴ M, the maximum adsorption took place for AC-SDSS. Initially, adsorption was slow and increases with increase in contact time and then reaches the saturation [52]. This is clearly depicted in Fig. 9. Figure 8 shows the % adsorption of CO₂ vs adsorbent dose for AC-WSS. When the adsorbent dosage was raised from 0.030 to 0.210 g at a fixed concentration of 5 × 10⁻⁴ M with a contact time of 70 min, maximum CO₂ adsorption was found to be 93%. It inferred a quick breakthrough speed that may be due to the quicker diffusivity and the minimum equilibrium adsorption as suggested by Tobameekul *et al.* [55]. Figure 8 shows that when the dosage of AC-WSS was set to 0.150 g with concentrations of 4 × 10⁻⁴, 5 × 10⁻⁴, and 6 × 10⁻⁴ M, maximum adsorption occurred during a contact period of 70 min at concentration 5 × 10⁻⁴ M. This could be due to the abundance of active sites available for the CO₂ molecule to settle in and become adsorbed. Falco and groups and Yoro *et al.* [56, 57] obtained a similar outcome.

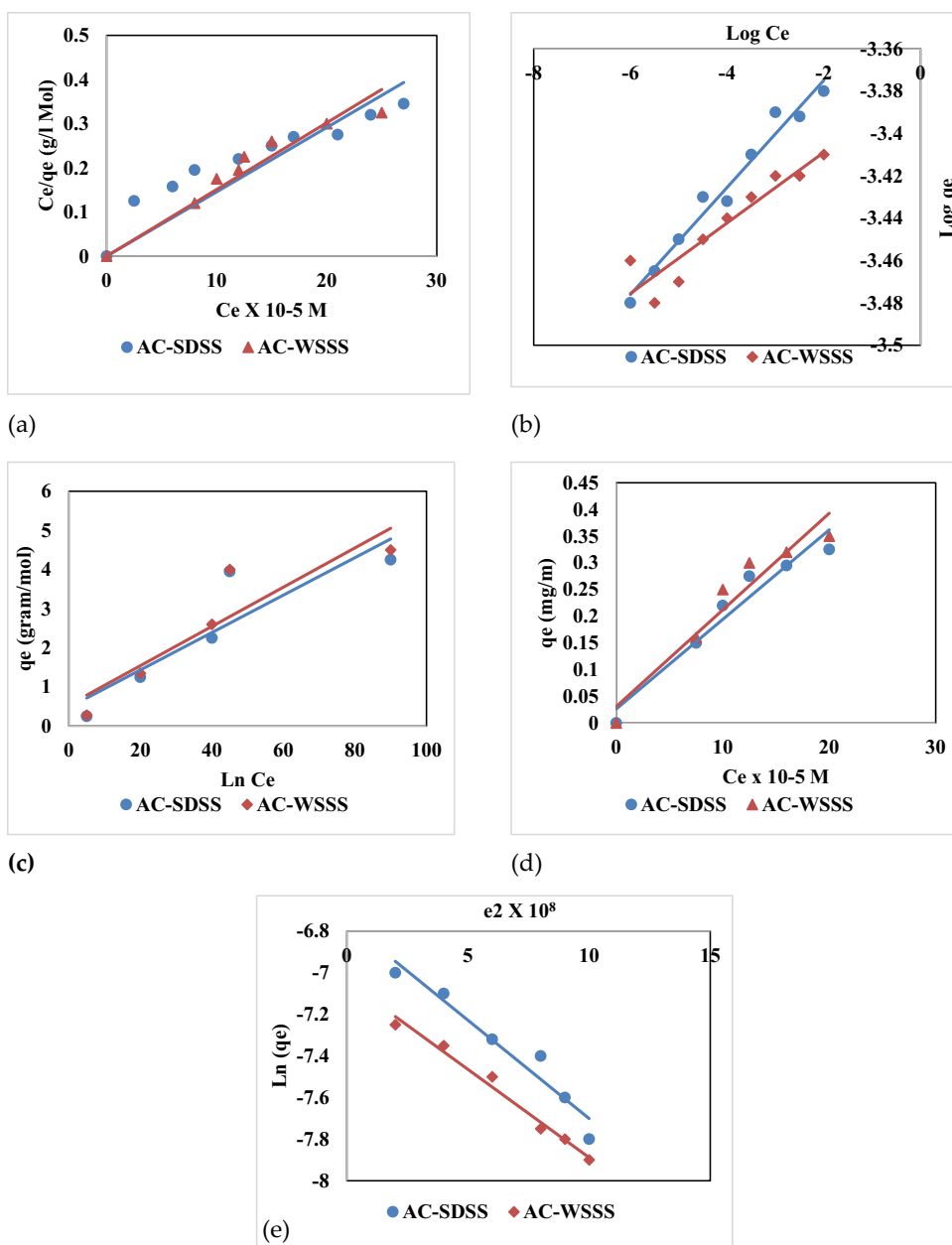
4.3 Sorption isotherm modeling

Models described in section 3.2 were used in the modeling of CO₂ sorption using AC-WSS and AC-SDSS. Le Chatelier’s principle, which states that endothermic desorption is preferable at higher temperatures, explains the decrease in CO₂ adsorption capacity. The CO₂ adsorption exothermic nature is mirrored by the *q_m* value, which tends to decrease as the adsorption temperature rises. A separation factor can also be used to determine the favorability of an adsorption process. A *R_L* value in the range of 0–1 indicates that CO₂ adsorption is favorable [54, 58]. Furthermore, the Freundlich constant, *n*, which is within the range of 1–2 as indicated in Table 2, supports the favorability of CO₂ adsorption. The Dubinin-Radushkevich and Temkin isotherms will also provide important information about energy parameters in terms of *E* (adsorption’s mean free energy) and *b_T* (adsorption’s heat) [59]. The Freundlich model provides better match to the experimental data over the whole temperature range based on *R²* value. As a result, it implies that the activated carbon surface is heterogeneous and that CO₂ adsorption happens in many layers rather than a monolayer, as proposed by the Langmuir type. Furthermore, Pérez and team [60] claimed that the Langmuir model best captures the chemisorption response

Table 2 Values of Adsorption isotherm models for different parameters of AC-SDSS

Isotherm	Parameters	Values	<i>R²</i>
Langmuir	<i>Q_m</i> (mol/g/min)	4.014 × 10 ⁻³	0.989
	<i>K_L</i> (g/mol)	6.73 × 10 ⁵	
	<i>R_L</i>	0.0085	
Freundlich	<i>K_F</i> (mol/g)	2.019 × 10 ⁻³	0.975
	<i>n</i>	1.2915	
Dubinin- Radushkevich	<i>Q_m</i> (mol/g/min)	1.0816 × 10 ⁻³	0.978
	<i>K</i> (mol ² /kJ ²)	5.748 × 10 ⁻³	
	<i>E</i> (kJ/mol)	43.82	
Temkin	<i>A_T</i> (L/g)	1.944 × 10 ⁻³	0.911
	<i>B</i> (kJ/mol)	7.64	
	<i>b_T</i>	59.64	
Sips	<i>q_m</i> (mg/g)	1.983 × 10 ⁻³	0.981
	<i>B</i> (kJ/mol)	0.19	
	<i>n</i>	0.98	

Fig. 11 **a** Langmuir adsorption isotherm of CO₂—AC-SDSS and AC-WSSS system. **b** Freundlich adsorption isotherm of CO₂—AC-SDSS and AC-WSSS system. **c** D-R adsorption isotherm of CO₂—AC-SDSS and AC-WSSS system. **d** Temkin adsorption isotherm of CO₂—AC-SDSS and AC-WSSS system. **e** Sips adsorption isotherm of CO₂—AC-SDSS and AC-WSSS system



due to the monolayer formation restriction, whereas the Freundlich model largely represents the physisorption process. In this work, the Langmuir isotherm model fits the concentration range studied far better than the other models.

Since R^2 values and adsorption capacity values for Freundlich, D-R, Temkin, and Sips models are lesser than the Langmuir model, the R_L value of 0.0085 confirms that CO₂ adsorption on AC-SDSS follows Langmuir model. A maximum mono-layer adsorption capacity of 4.014×10^{-3} mol/g/min was attained using Langmuir model. The values are given in Table 2 and are also checked with MATLAB for verification and found to be in accordance with the

calculated value. The isotherm plots for the CO₂ sorption was given in Fig. 11a–e.

In comparison to the other models, the Langmuir isotherm is the best fit based on adsorption capacity and R^2 values. Langmuir model's R_L was determined to be 0.0084, which is lower than unity which indicates a good adsorption. The slope and intercept of the plot between $\log q_e$ and $\log C_e$ are used to derive K_F and n values for the Freundlich model. The K_F value is 6.435×10^{-3} mol/g, and the n value is 2.55, indicating that CO₂ adsorption on the adsorbent is superior [49]. The surface area is heterogeneous, allowing for multi-layer CO₂ adsorption and physical adsorption. It

Table 3 Values of adsorption isotherm models for different parameters of AC-WSSS

Isotherm	Parameters	Values	R^2
Langmuir	Q_m (mol/g/min)	5.034×10^{-3}	0.9855
	K_L (g/mol)	5.12×10^4	
	R_L	0.0084	
Freundlich	K_F (mol/g)	6.435×10^{-3}	0.9805
	n	2.55	
Dubinin-Radushkevich	Q_m (mol/g/min)	2.014×10^{-3}	0.974
	K (mol ² /kJ ²)	2.135×10^{-3}	
	E (kJ/mol)	10.85	
Temkin	A_T (L/g)	2.055×10^{-3}	0.954
	B (kJ/mol)	1.52	
	b_T	49.645	
Sips	q_m (mg/g)	3.12×10^{-3}	0.957, 0.943
	B (kJ/mol)	0.21	

Table 4 Thermodynamic values for AC-SDSS system

Temperature, K	ΔG° (KJ/mol)	ΔH° (KJ/mol)	ΔS° (KJ/mol K)
303	-7.48	-48.57	36.44
313	-5.65		
323	-4.24		

also has a higher R^2 value of 0.9895, indicating that it is the best among all the models. The values are listed in Table 3.

4.4 Thermodynamic properties for AC-SDSS

From Van't Hoff equation, standard enthalpy and entropy were determined as suggested by Balsamo and group [9]. From the plot of $\ln K$ Vs $1/T$, slope and intercept gives ΔH° and ΔS° values, and they are listed in Table 4. At 303 K, 313

K, and 323 K, the effect of temperature on adsorption of CO_2 on AC-SDSS and AC-WSSS was studied.

Table 4 lists the estimated values for the thermodynamic parameters. The negative sign of the ΔH° value, based on the experimental observations, implies that the CO_2 adsorption process is exothermic. So, it may be deduced from the behavior of CO_2 molecules during the adsorption process, which transitions from a randomized to an ordered state on the adsorbent surface. The fall in entropy value during the adsorption process is due to the gas molecule having a lower degree of freedom due to the carbon surface having a limited amount of free space [34]. Furthermore, the quantity of ΔH° indicates the sort of CO_2 adsorption process, whether it is physical adsorption or chemical adsorption. The magnitude of ΔH° for the physisorption reaction has been reported to be less than 20 kJ/mol; therefore, the computed ΔH° of 48.57 kJ/mol indicates that it is chemisorption. The ΔG° values, on the other hand, imply the occurrence of favorable and spontaneous adsorption. Furthermore, because the negative ΔG° value decreases with increasing temperature, the CO_2 adsorption process is more favorable at 303 K than at 323 K [58].

Negative ΔG° suggests the spontaneous reaction [54]. ΔH° value was found to be -48.57 KJ/mole which is greater than -40 KJ/mol [61]. These results support that CO_2 adsorption on AC-SDSS is chemisorption. ΔS° value of 36.44 KJ/mol K indicates the affinity of adsorbents for CO_2 . Thermodynamic plot is given in Fig. 12.

At three distinct temperatures, 303 K, 313 K, and 323 K, the influence of temperature on CO_2 adsorption on adsorbent was investigated. As the temperature raises, the value of ΔG° decreases, indicating a decrease in CO_2 adsorption capability, and adsorption was more favorable at 303 K. Nor Adilla and team [54] argued that a negative Gibb's free energy shift indicates a spontaneous reaction. Furthermore, the amount of ΔH° reflects the type of CO_2 adsorption method, such as physical or chemical adsorption. At 303 K,

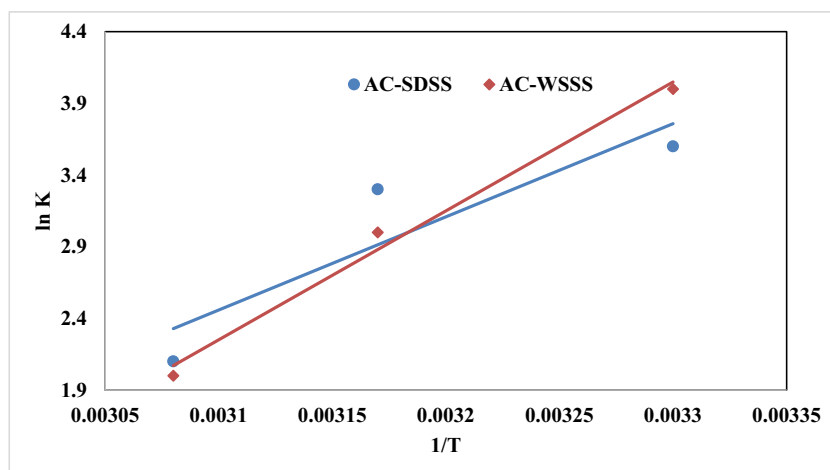
Fig. 12 Thermodynamic study of CO_2 —AC-SDSS and AC-WSSS system

Table 5 Thermodynamic values for AC-WSSS system

Temperature, K	ΔG° (KJ/mol)	ΔH° (KJ/mol)	ΔS° (KJ/mol K)
303	-7.45	-13.66	38.32
313	-6.95		
323	-5.12		

the calculated change in enthalpy ΔH° is -13.66 kJ/mol, which is less than Zhao and Liang's [61, 62] proposed value of -40 kJ/mol. CO_2 adsorption on AC-WSSS is a physical adsorption, and the entropy ΔS° is 38.32 kJ/mol K, indicating adsorbent affinity for CO_2 . Values are given in Table 5, and plot is given by Fig. 12.

4.5 Kinetic studies for adsorption of CO_2

Fast adsorption kinetics is one of the most important features expected for a good adsorbent, because the residence time necessary to complete the adsorption process, adsorption bed size, and, as a result, unit capital expenditures are all integrally linked to the rate of adsorption.

The pseudo-first order model overestimates CO_2 uptake in the early phases of adsorption and underestimates it as the equilibrium approaches. Nonetheless, the pseudo-first order prediction closely follows the patterns of the experimental data during the last phases of adsorption, and the equilibrium CO_2 adsorption capacities are in good agreement with the experimental values.

The pseudo-second order model, on the other hand, overestimates CO_2 uptake in the early stages while underestimating it in the latter stages since it predicts considerably lower equilibrium adsorption capabilities than the experimental values. Diffusion-based effects may be highly essential for porous adsorbents like activated carbons; hence, the physical

relevance of the evaluated rate constants must be carefully determined to acquire an accurate understanding of the mass transfer mechanisms involved. Using an intra-particle diffusion model, the possibility of intra-particle diffusion resistance affecting CO_2 adsorption on the evaluated activated carbons was investigated.

Assumption is made in pseudo-first order equation that the adsorption rate is based on adsorption capacity [34]. Slope and intercept of plot between $\log(q_e - q_t)$ Vs t gives k_1 and q_e values, respectively. Also, plots are straight line for different concentrations, and the values are reported in Table 6. The pseudo-second-order model states that chemisorption is the controlling mechanism with involvement of valency forces by electron sharing between the adsorbent and adsorbate [34]. The values of II order parameter are given in Table 6.

The R^2 value for intra particle diffusion model of 0.923 is less when compared to pseudo II order. Pronounced deviation was also observed in the graphs for intra particle diffusion model. With increasing CO_2 concentration, values of II order rate constant and equilibrium adsorption capacity decrease. R^2 values are found to be 0.988, which reveals that adsorption of CO_2 on adsorbent is due to chemical adsorption [35]. Also, experimental and calculated q_e values are in accordance with our study which further confirms that adsorption of CO_2 on AC-SDSS follows pseudo II order reaction [63]. Figure 13a–c represents the plot for kinetics of CO_2 adsorption for PFO, PSO, and intra-particle diffusion models.

The sorbent capacity of AC-WSSS was calculated using sorption capacity at equilibrium (q_e) [64]. Table 7 shows that as the concentration of adsorbate increases, the rate constant decreases, and the R^2 value approaches unity (0.9882). The computed q_e values are in good agreement with experimental data, indicating that the CO_2 adsorption kinetics on AC-WSSS follows pseudo II order kinetics. Figure 14a–c

Table 6 Kinetic parameters for adsorption of CO_2 on AC-SDSS

Kinetic models	Concentrations		
	4.0×10^{-4} M	5.0×10^{-4} M	6.0×10^{-4} M
Pseudo I order			
Experimental q_e (mol/g/min)	3.245×10^{-4}	3.218×10^{-4}	3.981×10^{-4}
Calculated q_e (mol/g/min)	1.06×10^{-4}	2.33×10^{-4}	2.72×10^{-4}
k_1 (1/min)	0.081	0.082	0.091
R^2	0.967		
Pseudo II order			
Calculated q_e (mol/g/min)	3.81×10^{-4}	3.95×10^{-4}	4.22×10^{-4}
K_2 (1/min)	12.71×10^2	11.68×10^2	9.96×10^2
R^2	0.988		
Intra particle diffusion			
K_{ipd} (g/mol.min ^{0.5})	0.0388	0.0538	0.0679
C	1.09	1.25	1.76
R^2	0.923		

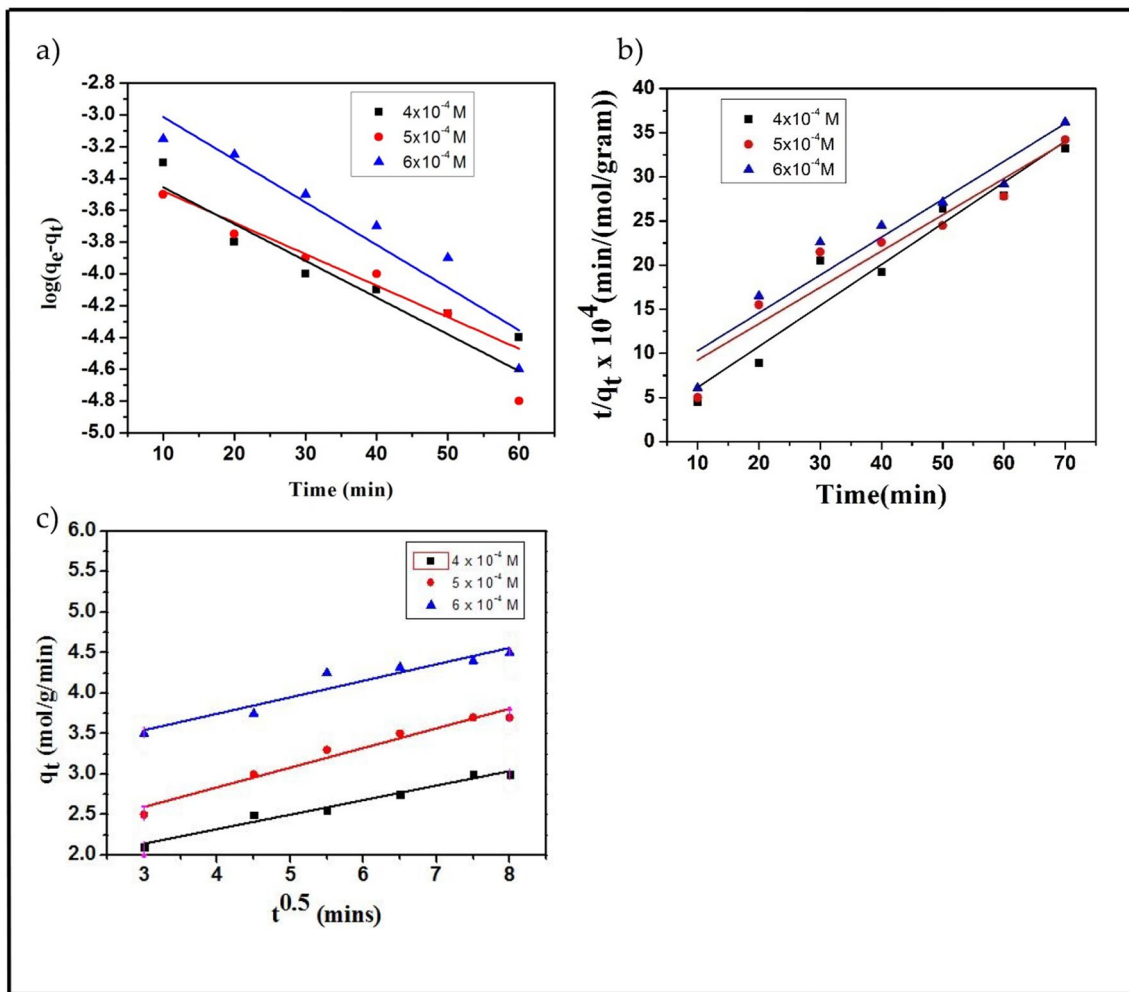


Fig. 13 a Pseudo I order adsorption of CO₂ on AC-SDSS system. b Pseudo II order adsorption of CO₂ on AC-SDSS system. c Intra-particle diffusion model

Table 7 Kinetic parameters for adsorption of CO₂ on AC-WSSS

Kinetic models	Concentrations		
	4.0 × 10 ⁻⁴ M	5.0 × 10 ⁻⁴ M	6.0 × 10 ⁻⁴ M
Pseudo I order			
Experimental <i>q_e</i> (mol/g/min)	3.435 × 10 ⁻³	3.785 × 10 ⁻³	4.1 × 10 ⁻³
Calculated <i>q_e</i> (mol/g/min)	1.01 × 10 ⁻³	2.1 × 10 ⁻⁴	2.42 × 10 ⁻⁴
<i>k₁</i> (1/min)	0.083	0.071	0.065
<i>R</i> ²	0.9742		
Pseudo II order			
Calculated <i>q_e</i> (mol/g/min)	3.91 × 10 ⁻³	3.65 × 10 ⁻³	4.05 × 10 ⁻³
<i>K₂</i> (1/min)	1.21 × 10 ²	1.12 × 10 ²	1.01 × 10 ²
<i>R</i> ²	0.9882		
Intra-particle diffusion			
<i>K_{ipd}</i> (g/mol.min ^{0.5})	0.0488	0.0589	0.8764
<i>C</i>	1.29	1.46	1.98
<i>R</i> ²	0.954		

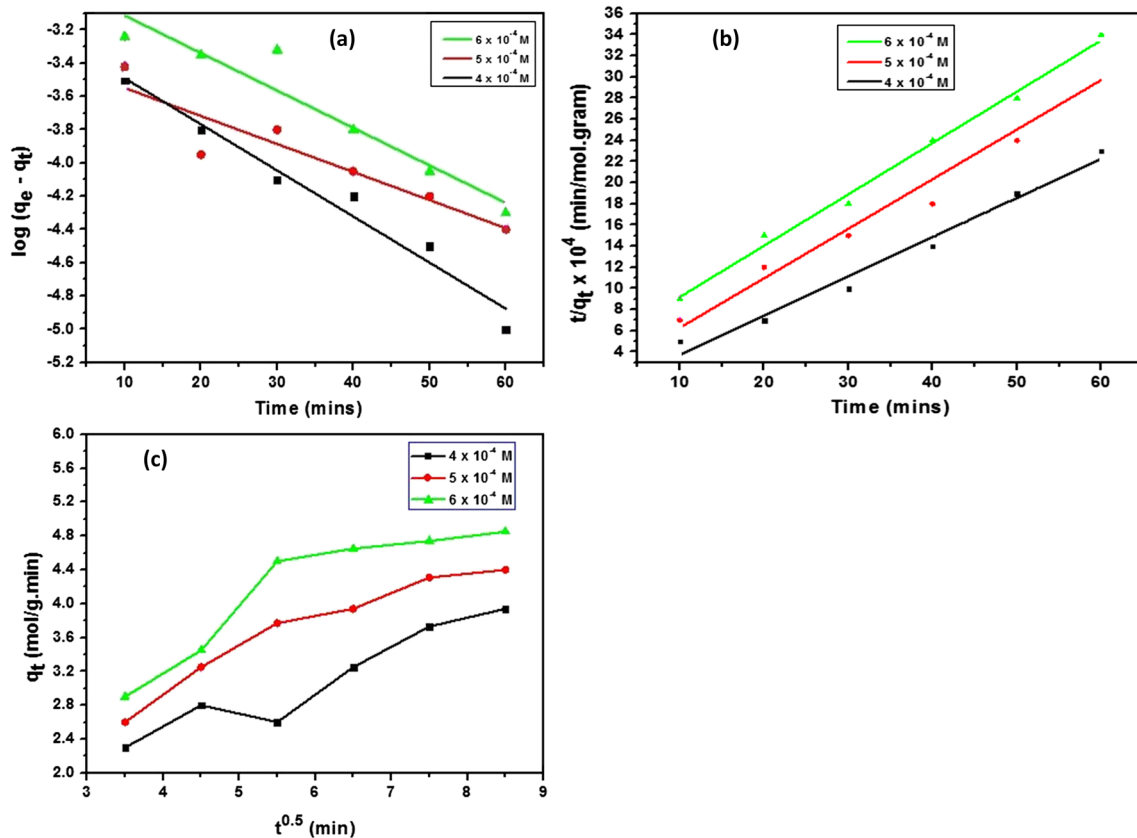


Fig. 14 **a** Pseudo I order adsorption of CO₂ on AC-WSSS system. **b** Pseudo II order adsorption of CO₂ on AC-WSSS system. **c** Intra-particle diffusion model

represents the plot for kinetics of CO₂ adsorption for PFO, PSO, and intra-particle diffusion models.

For the external barrier to mass transfer around the particles in the intra-particle diffusional model, only the early stages of adsorption are considered relevant. The common adsorption processes are covered in the second linear segment, which is regulated by intraparticle diffusion. Because the plots do not travel through the origin, pore diffusion cannot be the only rate-limiting process.

5 Adsorption of AC-SDSS and AC-WSSS towards CO₂

In general, the specific surface area (SSA) and the micropore volume have a strong relationship with gas adsorption ability. During the adsorption process, when gas molecules are adsorbed into the porous surface of the adsorbent, the van der Waals forces of attraction between the gas molecules cause this. It is thought that the strongest gas adsorption behavior will be seen in pores with sub-nanometer ranges, as they begin to overlap with pore size reduction. The formation

of deep potential wells also results in a significantly larger binding energy [40]. As a result, increasing the number of sub-nanometer holes is critical since it improves the SSA for adsorption automatically. The most important component of achieving high adsorption capacity performance is to produce adsorbents with improved pore architectures and CO₂ affinity [61]. The adsorption capacity of the sorbents synthesized in this work has superior uptake. The textural qualities of the synthesized AC-WSSS are excellent. Because the activated carbon was made from a combination of two materials, wild sugarcane and shrimp shells, the pore volume and surface area are as expected. Deep potential well development also results in a much higher binding energy [40]. As a result, increasing the number of sub-nanometer holes is crucial since it automatically increases surface area and pore volume. Producing adsorbents with better pore design and CO₂ affinity is the most important factor in achieving high adsorption capacity performance [6]. The comparative adsorption capacities of activated carbon synthesized from shrimp shells, sugar cane bagasse, and sawdust are tabulated in Table 8, and the adsorption capacity obtained from present work is higher and convincing comparatively.

Table 8 Adsorption capacities of activated carbon materials derived from sawdust, shrimp shells, and sugar cane bagasse materials

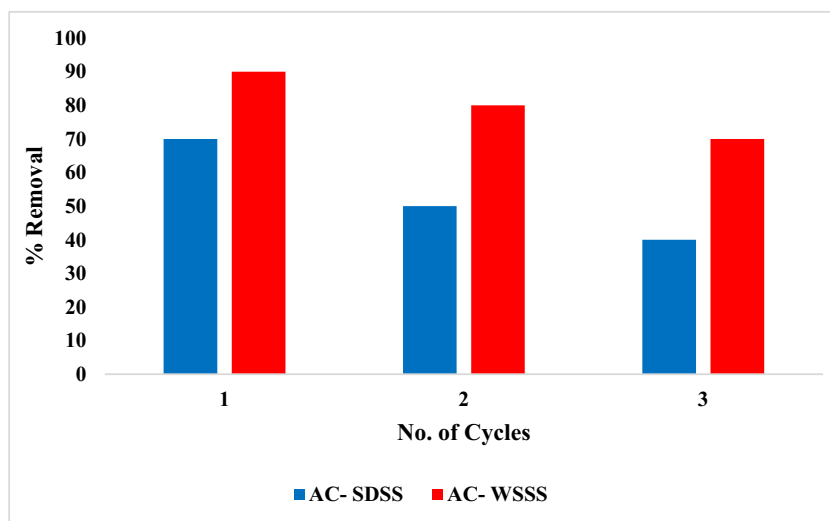
Materials	Adsorption capacity	References
Activated carbon from sawdust	3.6 mmol/g	[7]
Activated carbon from chitin aerogels	3.44 mmol/g (25 °C and 1 atm)	[65]
Activated carbon from pine sawdust	4.21 mmol/g	[66]
Sawdust biochar	0.47 kg CO ₂ /kg biochar	[25]
Activated carbon from agricultural residues	1.79 mmol/g	[18]
Activated carbons prepared from Eucalyptus camaldulensis wood	4.10 mmol/g	[67]
Activated carbon produced from paulownia sawdust	8.0 mmol/g	[68]
Activated carbon from honeycomb monoliths	2.627–5.576 mmol/g ⁻¹	[69]
Activated carbon fibers	2.74 mmol/g	[70]
Porous carbon from shrimp shells	4.20 mmol/g (1 bar and 298 K)	[71]
Activated carbon from wild sugarcane and sawdust	5.936×10^{-3} mol/g	[40]
Activated carbon from shrimp shell	2.39–4.20 mmol/g at 298 K	[7]
Mesoporous-activated carbon from prawn shell hydrocarbonization	1.6 mg/g	[72]
Activated carbon form xerogels	4.9 mmol/g at 0 °C	[73]
N-doped activated carbon from sugarcane bagasse	4.8 mmol/g	[74]
Activated carbon from dates	4.07–6.40 mmol/g at 0 °C	[7]
Organic framework polymers	2.9 mmol/g at 0 °C	[75]
Activated carbon from polymers	4.61 mmol/g at 25 °C	[7]
KOH-activated carbon derived from raw molasses	5.4 mmol/g at 0 °C	[76]
This work	5.034×10^{-3} mol/g—AC-WSSS 4.014×10^{-3} mol/g—AC-SDSS	

6 Desorption studies of adsorbent

CO₂ adsorbed on adsorbent was desorbed by acetone to an extent of approximately 78.24%. With acetone as a desorption medium, maximum desorption took place [77, 78]. Also, it is evident that chemisorption is driving force for adsorbing CO₂ on adsorbate. It is observed that more than 80% of CO₂ is removed from acetone even after three cycles of desorption experiments. It is depicted in Fig. 15.

Acetone was used as the solvent for CO₂ desorption on AC-WSSS. The adsorbent left over after the procedure is combined with acetone in a 1:1.65 ratio, slightly heated to around 50 °C in a conical flask, and allowed to settle for half an hour. The CO₂ is absorbed by the adsorbent, which is then dried and put to use. According to Nor Adilla et al. [52], physical adsorption is the driving force for adsorbing CO₂ on adsorbate because it causes adsorbate molecules to build a subsequent layer onto the surface. Even after three

Fig. 15 Reusability of 0.150 g of AC-SDSS and AC-WSSS to remove CO₂ from 5×10^{-4} M aqueous solution



repetitions of the experiment, acetone was shown to remove roughly 94.2% of CO₂. It is depicted in Fig. 12.

7 Conclusions

The primary concern these days is global warming and the resulting changes in the climate brought about by human emissions of carbon dioxide (CO₂). The amount of CO₂ in the atmosphere has increased by more than 30% since the start of the industrial revolution, which has led to a number of disastrous events. In this work, adsorbent prepared from sawdust, shrimp waste, and sugarcane waste by activation process served as best adsorbent for CO₂ adsorption. Optimum conditions of variables were found for CO₂ sorption of both sorbents. EDAX revealed that there is an interaction of CO₂ on the surface of the activated carbon with increase in carbon ratio. Chemisorption is a driving force for adsorption of CO₂ on the adsorbent. Equilibrium adsorption data was fitted with Langmuir adsorption isotherm, and monolayer adsorption capacity of CO₂ was found to be 5.034×10^{-3} mol/g and 4.014×10^{-3} mol/g for the sorbent activated carbon-wild sugar cane shrimp shells (AC-WSSS) and activated carbon-sawdust shrimp shells (AC-SDSS), respectively. The results suggest that the sorption of CO₂ follows pseudo II order kinetics. The peak shift seen in the FTIR after adsorption confirms that it follows chemisorption. The sorbents used in this work are regenerated using acetone as desorbing medium and found that they can be used for 3 cycles. From the results obtained, it can be concluded that the synthesized adsorbents AC-SDSS and AC-WSSS can be successfully employed in removing pollutants from various gas streams. These adsorbent AC-SDSS and AC-WSSS are suitable due to its renewability and economically feasible in nature. The results obtained in this study can serve as a benchmark while designing an adsorption-based gas storage system.

Acknowledgements The authors are thankful to Department of Petrochemical Technology, UCE, BIT Campus, Anna University, Tiruchirappalli, Tamil Nadu, 620024, India for the technical support provided.

Author contribution KK had the idea for the article. All authors contributed to the literature search and data analysis. The first draft of the manuscript was written by LN, and all authors commented and critically revised the work. All authors read and approved the final manuscript.

Data availability The dataset generated and/or analyzed during the current study are available from the corresponding author (L. Nagarajan) upon reasonable request.

Declarations

Ethics approval and consent to participate Not applicable.

Consent of publication Not applicable.

Competing interests The authors declare no competing interests.

References

- Wei M, Yu Q, Xie H, Zuo Z, Hou L, Yang F (2017) Kinetics studies of CO₂ adsorption and desorption on waste ion-exchange resin-based activated carbon. *Int J Hydrog Energy* 42:27122–27129
- Songolzadeh M, Ravanchi MT, Soleimani M (2012) Carbon dioxide capture and storage: a general review on adsorbents. *Int J Chem Mol Eng* 6:10
- Allen CD, Macalady AK, Chenchouni H, Bachelet D, McDowell N, Vennetier M, Kitzberger T, Rigling A, Breshears DD, Hogg ET (2010) A global overview of drought and heat-induced tree mortality reveals emerging climate change risks for forests. *For Ecol Manag* 259:660–684. <https://doi.org/10.1016/j.foreco.2009.09.001>
- Rashidi NA, Yusup S (2017) Potential of palm kernel shell as activated carbon precursors through single stage activation technique for carbon dioxide adsorption. *J Clean Prod* 168:474–486. <https://doi.org/10.1016/j.jclepro.2017.09.045>
- Ahmed MB, Johir MAH, Zhou JL, Ngo HH, Nghiem LD, Richardson C, Moni MA, Bryant MR (2019) Activated carbon preparation from biomass feedstock: clean production and carbon dioxide adsorption. *J Clean Prod* 225:405–413
- Serafin J, Narkiewicz U, Morawski AW, Wrobel RJ, Michalkiewicz B (2017) Highly microporous activated carbons from biomass for CO₂ capture and effective micropores at different conditions. *J CO₂ Util* 18:73–79
- Serafin J, Baca M, Biegun M, EwaMijowska RJ, Kaleńczuk J-N, Michalkiewicz B (2019) Direct conversion of biomass to nanoporous activated biocarbons for high CO₂ adsorption and supercapacitor applications. *Appl Surf Sci* 497:143722
- Yang N, Wang R (2015) Sustainable technologies for the reclamation of greenhouse gas CO₂. *J Clean Prod* 103:784–792. <https://doi.org/10.1016/j.jclepro.2014.10.025>
- Balsamo M, Budinova T, Erto A, Lancia A, Petrova B, Petrov N, Tsyntarski B (2014) Kinetic, thermodynamic and regeneration studies for CO₂ adsorption onto activated carbon. *Int J Adv Mech Eng* 4(1):27–32
- Dabrowski A (2011) Adsorption from theory to practice. *Adv Colloid Interf Sci* 93:135–224
- Guo B, Chang L, Xie K (2006) Adsorption of carbon dioxide on activated carbon. *J Nat Gas Chem* 15:223–229
- Dwiyaniti M, Elang Barruna AG, Muhamad Naufal R, Subiyanto I, Setiabudy R, Hudaya C (2020) Extremely high surface area of activated carbon originated from sugarcane bagasse. *Mater Sci Eng* 909:012018. <https://doi.org/10.1088/1757-899X/909/1/012018>
- Rocha PD, Franca AS, Oliveira LS (2015) Batch and column studies of phenol adsorption by an activated carbon based on acid treatment of corn cobs. *Int J Eng Technol* 7(6):459–464
- Adio SO, Ganiyu SA, Usman M, Abdulazeez I, Alhooshani K (2020) Facile and efficient nitrogen modified porous carbon derived from sugarcane bagasse for CO₂ capture: experimental and DFT investigation of nitrogen atoms on carbon frameworks. *Chem Eng J* 382:122964
- Rocha PD, Franca AS, Oliveira LS (2017) Batch and column studies of phenol adsorption by an activated carbon based on acid treatment of corn cobs. *Int J Eng Technol* 7(6)
- Nazir G, Rehman A, Park SJ (2021) Valorization of shrimp shell biowaste for environmental remediation: efficient contender for CO₂ adsorption and separation. *J Environ Manag* 299(1):113661

17. Rashidi NA, Yusup S, Borhan A (2014) Development of novel low cost activated carbon for carbon dioxide capture. *Int J Chem Eng Appl* 5(2):90–94
18. Demiral H, Demiral İ, Karabacakoglu B, Tımsek F (2011) Production of activated carbon from olive bagasse by physical activation. *Chem Eng Res Des* 89:206–213
19. Sutrisno B, Rizka NA, Hidayat AS, Hidayat A (2016) Preparation and characterization of activated carbon from sugarcane bagasse by physical activation with CO₂ gas. *Mater Sci Eng* 105:012027
20. Saxena R, Vinod Kumar Singh E, Kumar A (2014) Carbon dioxide capture and sequestration by adsorption on activated carbon. *Energy Procedia* 54:320–329
21. Jiang W, Zhang L, Guo X, Yang M, Lu Y, Wang Y, Zheng Y, Wei G (2021) Adsorption of cationic dye from water using an iron oxide/activated carbon magnetic composites prepared from sugarcane bagasse by microwave method. *Environ Technol* 42(3):337–350
22. Ogungbenro AE, Quang DV, Al-Ali KA, Vega LF, Mohammad RM, Zahra A (2020) Synthesis and characterization of activated carbon from biomass date seeds for carbon dioxide adsorption. *J Environ Chem Eng* 8(5):104257
23. Dubinin MM (1960) The potential theory of adsorption of gases and vapors for adsorbents with energetically non-uniform surface. *Chem Rev* 60:235–266
24. Madzakia H, Wan Azlina Wan AB, Ghania K, Rebitanima NZ, Aliasb AB (2016) Carbon dioxide adsorption on sawdust biochar. *Procedia Eng* 148:718–725
25. Mochizuki Y, Bud J, Byambajav E, Tsubouchi N (2022) Preparation and evaluation of activated carbon from low-rank coal via alkali activation and its fundamental CO₂ adsorption capacity at ambient temperature under pure pressurized CO₂. *React Chem Eng* 7:1429–1446
26. Guo Y, Tan C, Sun J, Li W, Zhang J, Zhao C (2020) Porous activated carbons derived from waste sugarcane bagasse for CO₂ adsorption. *Chem Eng J* 381:122736
27. Qin F, Li J, Zhang C et al (2022) Biochar in the 21st century: a data-driven visualization of collaboration, frontier identification, and future trend. *Sci Total Environ* 818:151774. <https://doi.org/10.1016/j.scitotenv.2021.151774>
28. Langmuir I (1916) The adsorption of gases on plane surface of glass, mica and platinum. *J Am Chem Soc* 40:1361–1368
29. Coromina HM, Walsh DA, Mokaya R (2016) Biomass-derived activated carbon with simultaneously enhanced CO₂ uptake for both pre and post combustion capture applications. *J Mater Chem A* 4:280–289
30. Sevilla MB, Fuertes A (2011) Sustainable porous carbons with a superior performance for CO₂ capture. *Energy Environ Sci* 4:1765–1771. <https://doi.org/10.1039/C0EE00784F>
31. Parshetti GK, Chowdhury S, Balasubramanian R (2015) Biomass derived low-cost microporous adsorbents for efficient CO₂ capture. *Fuel* 148:246–254. <https://doi.org/10.1016/j.fuel.2015.01.032>
32. Guangzhi Y, Jinyu Y, Yuhua Y et al (2017) Preparation and CO₂ adsorption properties of porous carbon from camphor leaves by hydrothermal carbonization and sequential potassium hydroxide activation. *RSC Adv* 7:4152–4160. <https://doi.org/10.1039/C6RA25303B>
33. Alghamdi AA, Al-Odayni AB, Saeed WS, Al-Kahtani A, Alharthi FA, Aouak T (2020) Efficient adsorption of lead (II) from aqueous phase solutions using polypyrrole-based activated carbon. *Materials (Basel)* 12(12):2020. <https://doi.org/10.3390/ma12122020>
34. Wu X, Zhang C, Tian Z, Cai J (2018) Large-surface-area carbons derived from lotus stem waste for efficient CO₂ capture. *New Carbon Mater* 33:252–261. [https://doi.org/10.1016/S1872-5805\(18\)60338-537](https://doi.org/10.1016/S1872-5805(18)60338-537)
35. Rashidi NA, Yusup S, Lam HL (2013) Kinetic studies on carbon dioxide capture using activated carbon. *Chem Eng Trans* 35:361–366
36. Zafaneli LFAS, Henrique A, Stedinger H, Tuesta JL, Gläsel J, Rodrigues AE, Gomes ET, Etzold BJM, Silva JAC (2022) D-printed activated carbon for post-combustion CO₂ capture. *Micropor Mesopor Mater* 335:111818. <https://doi.org/10.1016/j.micromeso.2022.111818>
37. Weber WJ, Morris JC (1963) Kinetics of adsorption on carbon from solution. *J St Eng Div Am Soc Civ Eng* 89:31–38
38. Nunes CA, Guerreiro MC (2011) Estimation of surface area and pore volume of activated carbons by methylene blue and iodine numbers. *Quim Nova* 34:3
39. Nagarajan L, Sampath Kumar P, Arulraj A (2020) Solar assisted reduced graphene oxide as adsorbent for carbon dioxide and its kinetic studies. *Phys E Low Dimens Syst Nanostruct* 116(113739):41
40. Creamer AE, Gao B (2016) Carbon-based adsorbents for post combustion CO₂ capture: a critical review. *Environ Sci Technol* 50:7276–7289
41. Devnarain PB, Arnold DR, Davis SB (2002) Production of activated carbon from South African sugar cane bagasse. *Proc S Afr Sug Technol Ass* 76:477–489
42. Olugbenga SB, Mohd Azmier A, Tan TS (2011) Utilization of cocoa pod husk for the removal of Remazol black b. reactive dye from aqueous solutions: kinetic, equilibrium and thermodynamic studies. *Trends in Applied Sci Res* 6(8):794–812
43. Yin T, Liu D, Cai Y, Zhou Y (2019) Methane adsorption constrained by pore structure in high-rank coals using FESEM, CO₂ adsorption, and NMRC techniques. *Energy Sci Eng* 7(1):255–271
44. Kaur B, Gupta RK, Bhunia H (2019) Chemically activated nanoporous carbon adsorbents from waste plastic for CO₂ capture: breakthrough adsorption study. *Micropor Mesopor Mater* 282:146–158. <https://doi.org/10.1016/j.micromeso.2019.03.025>
45. Guo L-P, Zhang Y, Li W-C (2017) Sustainable microalgae for the simultaneous synthesis of carbon quantum dots for cellular imaging and porous carbon for CO₂ capture. *J Colloid Interface Sci* 493:257–264. <https://doi.org/10.1016/j.jcis.2017.01.00348>
46. Falco C, Marco-Lozar JP, Salinas-Torres D et al (2013) Tailoring the porosity of chemically activated hydrothermal carbons: influence of the precursor and hydrothermal carbonization temperature. *Carbon* 62:346–355. <https://doi.org/10.1016/j.carbon.2013.06.017>
47. Gonzalez JF, Silvia R, Gonzalez G, Carmen M, Nabais JM, Valente LA (2009) Porosity development in activated carbons prepared from walnut shells by carbon dioxide or steam activation. *Ind Eng Chem Res* 48:7474–7481
48. Hayet O, Najes G (2013) Removal of Cd (II) from phosphoric acid solution by adsorbents: equilibrium and kinetic studies. *Chem Sci Trans* 2:357
49. Peaiyeda AR, Tesi GO (2014) Sorption and desorption studies on toxic metals from brewery effluent using eggshell as adsorbent. *Adv Nat Sci* 7:15–24
50. Jayakumar R, Rajasimman M, Karthikeyan C (2015) Sorption and desorption of hexavalent chromium using a novel brown marine algae sargassum myriocystum. *Korean J Chem Eng* 32(10):2031–2046
51. Akpasi SO, Isa YM (2022) Effect of operating variables on CO₂ adsorption capacity of activated carbon, kaolinite, and activated carbon – kaolinite composite adsorbent. *Water-Energy Nexus* 5:21–28
52. Rashidi NA, Yusup S, Borhan A (2016) Isotherm and thermodynamic analysis of carbon dioxide on activated carbon. *Procedia Eng* 148:630–637
53. Boonchaauy A, Worathanakul P (2022) The diffusion behavior of CO₂ adsorption from a CO₂/N₂ gas mixture on zeolite 5A in a fixed-bed column. *Atmosphere* 13(4):513. <https://doi.org/10.3390/atmos13040513>
54. Baccile N, Titirici MM (2011) Morphological and structural differences between glucose, cellulose and lignocellulosic biomass derived hydrothermal carbons. *Green Chem* 13:3273–3281. <https://doi.org/10.1039/C1CG15742F>
55. Tobameekul P, Sangsuradet S, Worathanakul P (2022) Comparative study of Zn loading on advanced functional zeolite NaY

- from bagasse ash and rice husk ash for sustainable CO₂ adsorption with ANOVA factorial design. *Atmosphere* 13:314
56. De Falco M, Capocelli M, Basile A (2017) Selective membrane application for the industrial one-step DME production process fed by CO₂ rich streams: modeling and simulation. *Int J Hydrog Energy* 42(9):6771–6786
 57. Yoro KO, Amosa MK, Sekoai PT, Mulopo J, Daramola MO (2020) Diffusion mechanism and effect of mass transfer limitation during the adsorption of CO₂ in a packed-bed column. *Int J Sustain Eng* 13:54–67
 58. Monazam ER, Shadle LJ, Miller DC, Pennline HW, Fauth DJ, Hoffman JS, Gray MML (2013) Equilibrium and kinetics analysis of carbon dioxide capture using immobilized amine on a mesoporous silica. *AICHE J* 59:923–935
 59. Darvishi Cheshmeh Soltani R, Safari M, Rezaee A, Godini H (2015) Application of a compound containing silica for removing ammonium in aqueous media. *Environ Prog Sustain Energy* 34:105–111
 60. Pérez N, Sánchez M, Rincon G, Delgado L (2007) Study of the behavior of metal adsorption in acid solutions on lignin using a comparison of different adsorption isotherms. *Lat Am Appl Res* 37:157–162
 61. Zhao Y, Wang D, Xie H, Won SW, Cui L, Wu G (2015) Adsorption of Ag(I) from aqueous solution by waste yeast: kinetic, equilibrium and mechanism studies. *Bioprocess Biosyst Eng* 38:69–77
 62. Liang S, Guo X, Feng N, Tian Q (2010) Isotherms, kinetics and thermodynamic studies of adsorption of Cu²⁺ from aqueous solutions by Mg²⁺/K⁺ type orange peel adsorbents. *J Hazard Mater* 174:756–762
 63. Huang Y-T, Lee L-C, Shih M-C (2018) A study on pseudo-second-order kinetic equation for the adsorption of methylene blue onto nitric acid-treated rice husk. *Comparison of Linear methods*. *Int J Sci Res publ.* 8:2250–3153
 64. Aliakbarian B, Casazza AA, Perego P (2015) Kinetic and isotherm modelling of the adsorption of phenolic compounds from olive mill wastewater onto activated carbon. *Food Technol Biotechnol* 53:207–214
 65. Dassanayake RS, Gunathilaka C, Abidi N, Jaroniec M (2018) Activated carbon derived from chitin aerogels: preparation and CO₂ adsorption. *Cellulose* 25:1911–1920
 66. Quan C, Su R, Gao N (2020) Preparation of activated biomass carbon from pine saw dust for supercapacitor for CO₂ capture. *Int J Energy Res* 44(6):4335–4351. <https://doi.org/10.1001/er.5206>
 67. Heidari A, Rashidi A, Younesi H, Ghoreyshi AA (2014) Adsorptive removal of CO₂ on highly microporous activated carbons prepared from *Eucalyptus camaldulensis* wood: effect of chemical activation. *J Taiwan Inst Chem Eng* 45(2):579–588
 68. Zhu X-L, Wang P-Y, Peng C, Yang J, Yan X-B (2014) Activated carbon produced from paulownia sawdust for high-performance CO₂ sorbents. *Chin Chem Lett* 25(60):929–932
 69. Vargas DP, Giraldo L, Moreno-Piraján JC (2012) CO₂ adsorption on activated carbon honey comb-monoliths: a comparison of Langmuir and Toth models. *Int J Mol Sci* 13:8388–8397
 70. Chiang Y-C, Yeh C-Y, Weng C-H (2019) Carbon dioxide adsorption on porous and functionalized activated carbon fibers. *Appl Sci* 9:1977
 71. Yang F, Wang J, Liu L, Zhang P (2018) Synthesis of porous carbons with high N content from shrimp shells for efficient CO₂ capture and gas separation. *ACS Sustain Chem Eng* 6:11
 72. Román S, Ledesma B, Álvarez-Murillo A, Sabio E, González JF, González CM (2016) Production of cost effective mesoporous materials from shell hydrocarbonization. *Nanoscale Res Lett* 11:435
 73. Martín-Jimeno FJ, Suárez-García F, Paredes JI, Martínez-Alonso A (2015) Activated carbon xerogels with a cellular morphology derived from hydrothermally carbonized glucose-graphene oxide hybrids and their performance towards CO₂ and dye adsorption. *Carbon* 81:137–147
 74. Han J, Zhang L, Zhao B, Qin L, Wang Y, Xing F (2019) The N-doped activated carbon derived from sugarcane bagasse for CO₂ adsorption. *Ind Crop Prod* 28:290–297
 75. Li T, Sullivan JE, Rosi NL (2013) Design and preparation of a core-shell metal-organic framework for selective CO₂ capture. *J Am Chem Soc* 135:9984–9987
 76. Kielbasa K, Kamińska A, Niedoba O, Michalkiewicz B (2021) CO₂ adsorption on activated carbons prepared from molasses: a comparison of two and three parametric models. *Materials* 14:7458
 77. Zeng W, Nai H (2016) Adsorption/desorption behaviors of acetone over micro-/mesoporous SBA-16 silicas prepared from rice husk agricultural waste. *Aerosol Air Qual Res* 16:2267–2277
 78. Li L, Sun Z, Li H, Keener TC (2012) Effects of activated carbon surface properties on adsorption of volatile organic compounds. *J Air Waste Manage Assoc* 62(10):2162–2906

Publisher's Note Springer Nature remains neutral with regard to jurisdictional claims in published maps and institutional affiliations.

Springer Nature or its licensor (e.g. a society or other partner) holds exclusive rights to this article under a publishing agreement with the author(s) or other rightsholder(s); author self-archiving of the accepted manuscript version of this article is solely governed by the terms of such publishing agreement and applicable law.